ELSEVIER

Journal of Wind Engineering
and Industrial Aerodynamics 92 (2004) 315–330

JOURNAL OF wind engineering AND industrial aerodynamics

www.elsevier.com/locate/jweia

An investigation of flow fields around flanged diffusers using CFD

Ken-ichi Abe[a,*], Yuji Ohya[b]

[a] *Department of Aeronautics and Astronautics, Kyushu University, Fukuoka 812-8581, Japan*
[b] *Research Institute of Applied Mechanics, Kyushu University, Kasuga 816-8580, Japan*

Received 14 August 2003; received in revised form 9 December 2003; accepted 10 December 2003

Abstract

Numerical investigations are carried out for flow fields around flanged diffusers to develop small-type wind turbines under 1.5 kW. In the calculations, an advanced closure approximation is adopted, within the framework of non-linear eddy-viscosity modeling, which aims specifically at an improved representation of turbulence anisotropy. Comparison of the computed results with the corresponding experimental data shows that the present calculation has the capability of providing reasonable predictions for the present complex turbulent flows. Furthermore, by processing the computational results, the input-power coefficient is estimated under various conditions of diffuser opening angle and loading coefficient. It is shown that the performance of a flanged diffuser strongly depends on the loading coefficient as well as the opening angle because it greatly affects the nature of the separation appearing inside the diffuser. The present investigation suggests that the loading coefficient for the best performance of a flanged diffuser is considerably smaller than that for a bare wind turbine.

Keywords: Wind turbine; Flanged diffuser; Input-power coefficient; Loading coefficient; Separation; Non-linear eddy-viscosity model

1. Introduction

The power in the wind is well known to be proportional to the cubic power of the wind velocity approaching a wind turbine. This means that even small amount of its acceleration gives large increase of the energy generation. Therefore, many research

*Corresponding author. Tel.: +81-92-642-3723; fax: +81-92-642-3752.
E-mail address: abe@aero.kyushu-u.ac.jp (K. Abe).

0167-6105/$ - see front matter
doi:10.1016/j.jweia.2003.12.003

groups have tried to find a way to accelerate the approaching wind velocity effectively [1–5]. Among them, some attractive studies were reported by Igra [1], Gilbert and Foreman [2], Nagai and Irabu [3] and Phillips et al. [4], regarding diffuser-augmented wind turbines.

Recently, on the other hand, Ohya et al. [6] have developed another kind of wind–acceleration system. Although it adopts a diffuser-shaped structure surrounding a wind turbine like the others [1–4], the feature that distinguishes it from the others is a large flange attached at the exit of diffuser shroud. Fig. 1 illustrates an overview of the present wind-acceleration system. Generally, a flange may be thought to be an obstacle against the flow coming smoothly. However, this flange generates large size of separation behind it, where a very low-pressure region appears to draw more wind compared to a diffuser with no flange. Owing to this effect, the flow coming into the diffuser can be effectively concentrated and accelerated. In this system, the maximum velocity is obtained near the inlet of diffuser and thus a wind turbine is located there as shown in Fig. 1. A simple design theory of wind turbine with flanged diffuser has also been developed by Inoue et al. [7], indicating that its design concept is very different from that for a bare wind turbine. Although a wind turbine designed by Inoue et al. [7] gives high performance in combination with a flanged diffuser, more detailed investigation about flow fields inside and periphery of diffuser is still needed to achieve the best performance.

Having considered the above background, in this study, several numerical investigations were carried out for flow fields around flanged diffusers. The computed results are compared with the corresponding experimental data to show the fundamental capability of predicting complex turbulent flows of this kind. Furthermore, by processing the computational results, the input-power coefficient is estimated under various conditions of diffuser opening angle and loading coefficient, with which we try to find a possible way of developing a small-type wind turbine with a flanged diffuser.

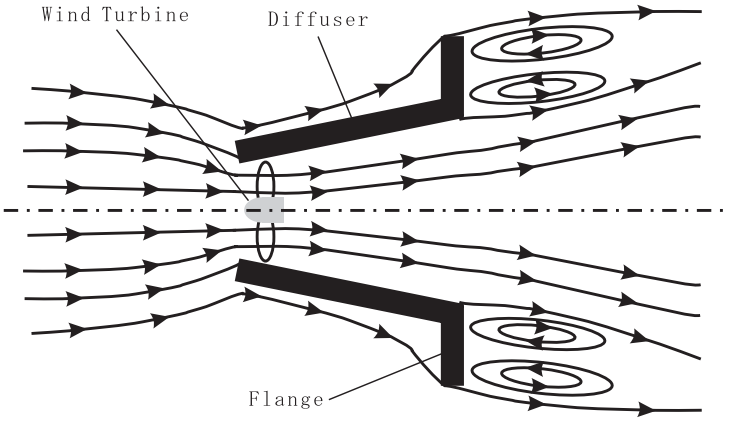

Fig. 1. Schematic view of flow mechanism around a flanged diffuser.

2. Numerical method and computational conditions

2.1. Governing equations and turbulence model

The present flow field is generally expressed by the continuity and the incompressible Reynolds-averaged Navier–Stokes equations as follows:

$$\frac{\partial U_i}{\partial x_i} = 0, \tag{1}$$

$$U_j \frac{\partial U_i}{\partial x_j} = -\frac{1}{\rho}\frac{\partial P}{\partial x_i} + \frac{\partial}{\partial x_j}\left\{ v\left(\frac{\partial U_i}{\partial x_j} + \frac{\partial U_j}{\partial x_i}\right) - \overline{u_i u_j} \right\} + F_i, \tag{2}$$

where $\overline{()}$ denotes Reynolds-averaged value. In Eq. (2), ρ, P, U_i, u_i and v, respectively, denote density, mean static pressure, mean velocity, turbulent fluctuation and kinematic viscosity. In the equation, F_i is the body-force term imposed for the representation of a load.

To predict complex turbulent flow fields in this study, the non-linear eddy-viscosity model proposed by Abe et al. [8] was adopted with some modifications for the length-scale equation. Although detailed descriptions of the algebraic expression for $\overline{u_i u_j}$ are given in the previous paper [8] and then dismissed here, it should be emphasized that this model provides good predictions for flow fields with massive separations [8,9].

In this model, the turbulence energy k is determined from the usual form of the transport equation:

$$U_j \frac{\partial k}{\partial x_j} = \frac{\partial}{\partial x_j}\left\{ \left(v + \frac{v_t}{\sigma_k}\right)\frac{\partial k}{\partial x_j} \right\} - \overline{u_i u_j}\frac{\partial U_i}{\partial x_j} - \varepsilon, \tag{3}$$

where ε is the dissipation rate of k. As for the length-scale variable, the original model proposed by Abe et al. [8] has two versions. One of them adopts ε (referred to as AJL-ε model) and the other introduces ω, which is specific dissipation rate of turbulence energy, i.e. $\omega \propto \varepsilon/k$ (referred to as AJL-ω model). Note that the last relation is used to extract ε from ω, which is required in the transport equation (3) and the model components [8].

So far, it has been said that the ω-equation tends to provide better results for the flow-field predictions with the adverse pressure gradient [10]. In fact, AJL-ω model provides better results than AJL-ε model for separated flows which are subjected to the strong adverse pressure gradient [8,9]. Although AJL-ω model has such an advantage, there still remains a crucial weakness that it gives a extremely large value in the vicinity of the wall and sometimes causes numerical stiffness. To reduce this numerical weakness, in this study, a new attempt was carried out to adopt another variable suited for the length-scale equation. This new parameter ψ is proportional to $\sqrt{\omega}$ and then its order becomes much smaller than that of ω. It may have the following formulation:

$$\psi = \frac{1}{\beta^*}\sqrt{\frac{\varepsilon}{k}}. \tag{4}$$

Note that Eq. (4) provides the means of extracting ε from ψ, which is required in the transport equation (3) and the model components to follow. A basic constitution of the transport equation for ψ can be derived from the transport equations for k and ε, followed by some effective modifications to improve the model performance. In this study, the final form of the ψ-equation is modeled as

$$U_j\frac{\partial\psi}{\partial x_j}=\frac{\partial}{\partial x_j}\left\{\left(\nu+\frac{\nu_t}{\sigma_\psi}\right)\frac{\partial\psi}{\partial x_j}\right\}+\alpha\tau S^2\psi-B\psi^3+E_\psi, \tag{5}$$

where

$$E_\psi=\{1-f_w(80)\}C_{\psi1}\tau\left(\frac{k}{\psi}\right)\frac{\partial\psi}{\partial x_j}\frac{\partial\psi}{\partial x_j}+\{1-f_w(600)\}C_{\psi2}\tau\frac{\partial k}{\partial x_j}\frac{\partial\psi}{\partial x_j},$$

$$\beta^*=\frac{\sqrt{\beta}+(R_{t\psi}/110)^4}{1+(R_{t\psi}/110)^4},\quad R_{t\psi}=\frac{k}{\nu\psi^2},\quad \tau=\frac{\nu_t}{k},$$

$$\nu_t=C_\mu f_\mu\frac{k^2}{\varepsilon},\quad \sigma_k=\frac{1.2}{f_t},\quad \sigma_\psi=\frac{0.75}{f_t},$$

$$f_\mu=\left[1+\frac{35}{R_t^{3/4}}\exp\left\{-\left(\frac{R_t}{30}\right)^{3/4}\right\}\right]\{1-f_w(26)\},\quad f_t=1+5.0f_w(5),$$

$$f_w(\xi)=\exp\left\{-\left(\frac{n^*}{\xi}\right)^2\right\},$$

$$C_\mu=0.12,\quad \alpha=0.29,\quad \beta=0.415,\quad C_{\psi1}=1.2,\quad C_{\psi2}=2.5. \tag{6}$$

In Eq. (6), $n^*(=(\nu\varepsilon)^{1/4}n/\nu)$ is the non-dimensional wall distance with the Kolmogorov velocity scale introduced [11,12] and ξ is a prescribed constant. Note that n is determined as the nearest distance from all the wall surfaces. The model coefficients for ψ-equation were calibrated in some representative test cases. The other model functions and model constants are the same as those of Abe et al. [8].

2.2. Computational conditions

The present computational conditions and grid system around a flanged diffuser are shown in Figs. 2 and 3, respectively. In this study, the flow was assumed to be an axisymmetric steady flow, with x and r being the streamwise and radial coordinates, respectively. In Fig. 2, L, D, ϕ and h, respectively, denote diffuser length, diffuser diameter at the inlet, diffuser opening angle and height of flange. The computational domain was determined not to give any serious problem to the obtained results. In fact, in the region far from the diffuser, the effect of blockage on the free stream was less than 2%. In Fig. 3, subscripts 0, 1, 2 and b denote values at the inlet (free stream), in front of the load (approaching), behind the load and at the exit of the diffuser, respectively. The load inside the diffuser was represented by the following

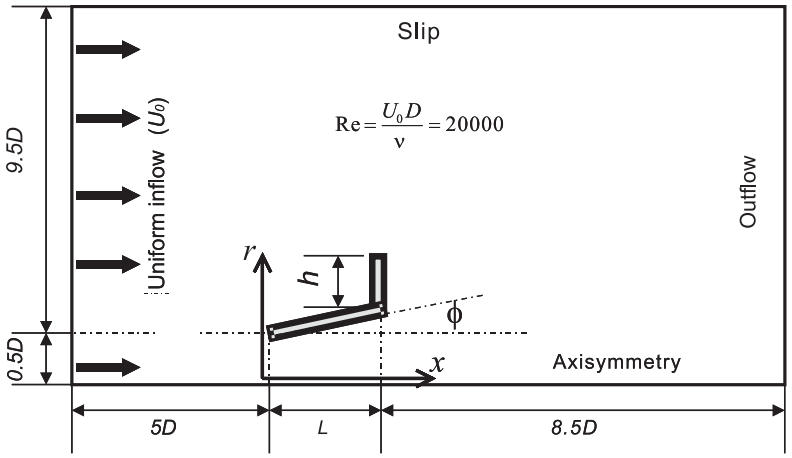

Fig. 2. Computational conditions.

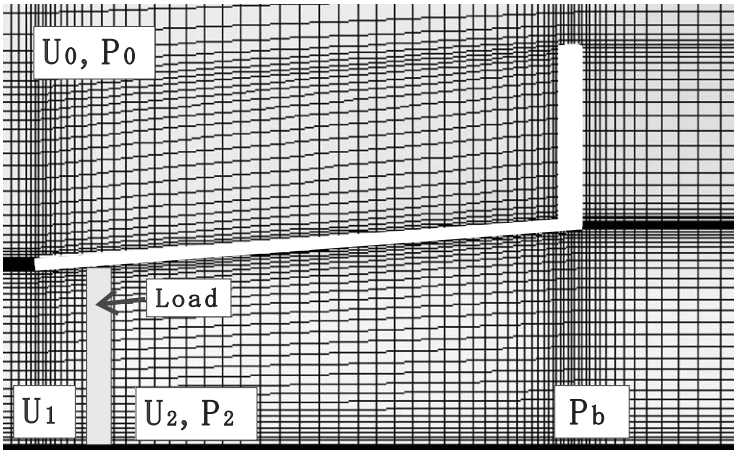

Fig. 3. Grid system.

general expression:

$$F_x = \frac{C_t}{\Delta}\frac{1}{2}U|U|, \quad F_r = 0, \tag{7}$$

where U is the streamwise velocity. In Eq. (7), C_t and Δ are the loading coefficient and its streamwise width imposed, respectively.

As for the inlet boundary condition, a uniform flow (U_0) with 3% of free stream turbulence was specified. At the outlet boundary, zero-streamwise gradients were prescribed. Concerning the top boundary, slip conditions were adopted. No-slip conditions were specified at the walls, where the nearest node was properly placed inside the viscous sublayer. The number of grid points in this study was 131×81. The Reynolds number ($Re = U_0 D/v$) was set to be 20000. Calculations were

performed with the finite-volume procedure STREAM of Lien and Leschziner [13], followed by several improvements and substantially upgraded by Apsley and Leschziner [14]. This method uses collocated storage on a non-orthogonal grid and all variables are approximated on cell faces by the UMIST scheme [15], a TVD implementation of the QUICK scheme. The solution algorithm is SIMPLE, with a Rhie-Chow interpolation for pressure.

The corresponding experimental data were taken by Ohya et al. [6]. A large boundary-layer wind tunnel was used at the Research Institute for Applied Mechanics, Kyushu University. It has a measurement section of 3.6 m (width) × 2 m (height) × 15 m (length) with the maximum wind velocity of 30 m/s. The diffuser model was hung and supported with strings in the center of the measurement section. In this experiment, the on-axis pressure was measured using a static pressure tube with the diameter of 3 mm. The on-axis streamwise velocity was measured using an I-type hot wire (for the results shown in Fig. 6) or evaluated from the pressure values measured by the aforementioned static pressure tube and a total pressure tube with the diameter of 3 mm (for the other results). The diameter at the inlet of the diffuser (D) was 0.2 m. The free stream velocity (U_0) was 5 m/s and then the Reynolds number based on the model diameter and the free stream velocity was 67 000. Although the Reynolds number is different between the computation and the experiment, it was confirmed from the experimental results that there was little Reynolds-number dependency at least in the present conditions. Note that the Reynolds-number dependency in the computational results will be discussed in the next section.

The present test cases are as follows. First, to examine the basic performance, computations were performed for various heights of flange ($h/D = 0 - 0.5$) with the condition of $L/D = 1.5$, $\phi = 4^\circ$ and $C_t = 0$ (no load) fixed. Next, to investigate the effect of loading coefficient, several computations were performed under various loading coefficients, with the condition of $L/D = 1.5$, $\phi = 4^\circ$ and $h/D = 0.5$ fixed. Finally, to show a possible direction of optimizing the performance of a flanged diffuser, another set of parameters, $L/D = 1.25$, $\phi = 15^\circ$ and $h/D = 0.35$, were examined and then the obtained results were compared with those of the other cases. For all the test cases, the load was imposed in the region of $x/D = 0.2 - 0.3$ (i.e. $\Delta = 0.1$) inside the diffuser.

3. Results and discussion

3.1. Basic performance of the present calculation

First, to assess the grid dependency and the Reynolds-number dependency of the computational results, Fig. 4 compares the on-axis distributions of streamwise velocity and pressure coefficient ($C_p = (P - P_0)/(\frac{1}{2}\rho U_0^2)$), under the condition of $L/D = 1.5$, $\phi = 4^\circ$, $h/D = 0.5$ and $C_t = 0$ (with no load). Two different grid numbers and two different Reynolds numbers were considered for comparison. As seen in the figure, the difference is very small between the results with two different

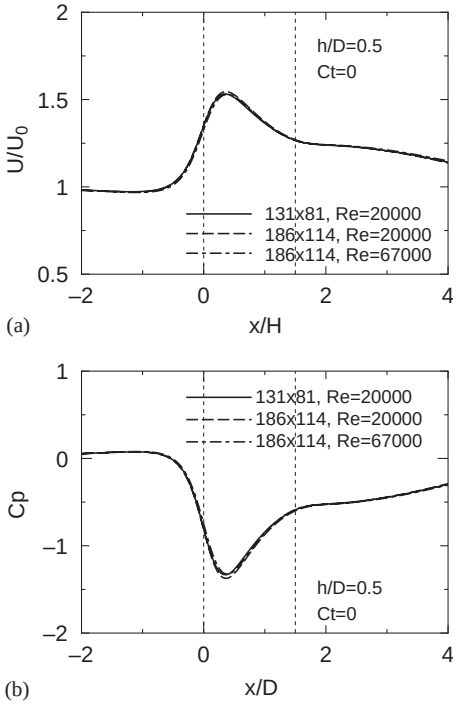

Fig. 4. Comparison of on-axis distributions ($L/D = 1.5$, $\phi = 4^\circ$, $C_t = 0$): (a) Streamwise velocity and (b) pressure coefficient.

grid numbers and thus it is found that the effect of grid dependency does not give any serious problem to the discussion on the flow fields. Also, as for the Reynolds-number dependency, the difference is very small between the results at two different Reynolds numbers. Therefore, it is understood that the lower Reynolds-number condition ($Re = 20\,000$) presently used does not cause any essential problem to investigate the flow fields in this study and it is practically useful to reduce the computational cost.

Streamlines and streamwise velocity contours for the same test case are shown in Fig. 5. It is seen that the streamlines smoothly flow inside the diffuser and the streamwise velocity does not change so much in the radial direction except for the boundary-layer region close to the diffuser wall. Considering this fact, it can be said that the on-axis distributions successfully explain the fundamental feature of the performance in such diffuser flows. Hence, in what follows, the diffuser performance is discussed mainly by using the on-axis values.

Figs. 6 and 7 compare the on-axis distributions of streamwise velocity and pressure coefficient, respectively, for various heights of flange under the condition of $L/D = 1.5$, $\phi = 4^\circ$ and $C_t = 0$ (with no load). The present results show reasonable trends for both on-axis velocity and pressure variations, though slight under-prediction is seen in the computational results inside the diffuser. In the region far

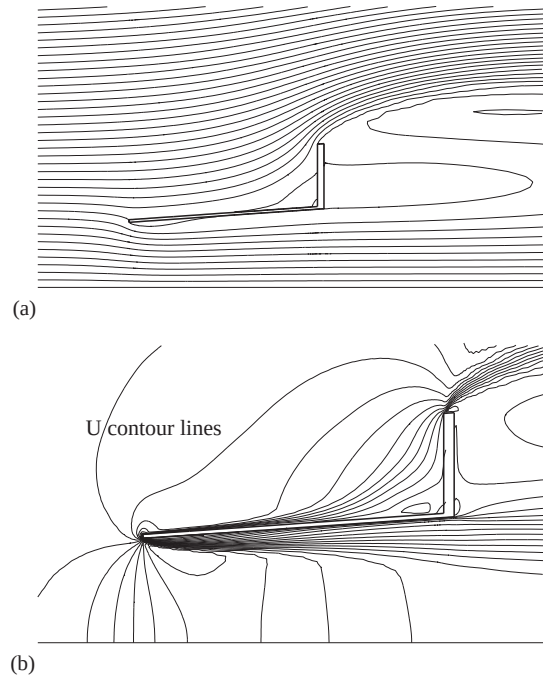

Fig. 5. Overview of flow field ($L/D = 1.5,\ \phi = 4^\circ,\ C_t = 0$): (a) Streamlines and (b) contour lines of streamwise velocity.

downstream of the diffuser exit, some difference is seen between the computational and the experimental results. In this region, the experimental results tend to show the decrease of the total pressure, while the computational results still show the aspect of the potential core. This fact may indicate that the turbulent wake behind the flange is more active in the experiment than in the computation. However, considering the fact that the characteristics of the flow field inside the diffuser are well captured and the effect of flange height is also reproduced properly, it can be thought that the aforementioned discrepancy in the downstream region gives no serious effect to the discussion on the performance of the flanged diffuser at least in this study.

From the figures, the acceleration mechanism of approaching flow can be understood. In a diffuser, the flow expands along the inside wall unless a massive flow separation occurs in the near-wall region, resulting in the increase of C_p and then the decrease of U toward the diffuser exit. As seen in the case with no flange ($h/D = 0$), they usually return to almost the same values as those of the surrounding flow (i.e. free stream values in this case). Due to this, the flow must accelerate in advance at the inlet to cover such a deceleration inside the diffuser. This is the reason why the approaching flow accelerates and the maximum velocity is obtained near the inlet.

Such being the case, the flow inside a diffuser has a strong connection with the surrounding flow. In this sense, a flange attached at the diffuser exit plays an

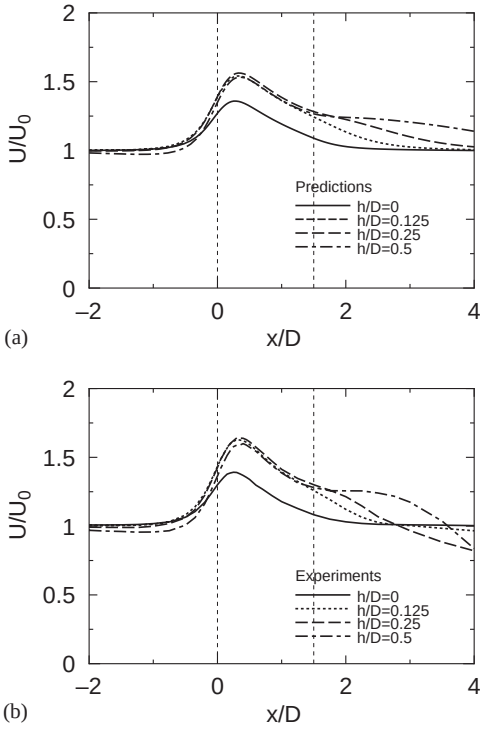

Fig. 6. Comparison of on-axis streamwise velocity ($L/D = 1.5$, $\phi = 4^\circ$, $C_t = 0$): (a) Predictions and (b) experiments.

important role to accelerate the approaching flow more effectively. As seen in Fig. 5, a flange generates a massive separation behind it, where a very low-pressure region appears. Owing to this, a much lower C_p is obtained at the diffuser exit ($x/D = 1.5$). On the other hand, the deceleration mechanism inside the flanged diffuser is similar to the case with no flange, so long as the same diffuser shape is used. Hence, under this condition, C_p inside the diffuser must return to a much lower value at the diffuser exit. Due to this restriction, the approaching flow must accelerate more to decrease C_p near the diffuser inlet, as is shown in the figures.

From these results, it can be said that the present computation sufficiently reproduces fundamental features of the flow fields of this kind. Also is found that the present computational results are very useful to investigate such flow fields in more detail.

3.2. *Effect of the loading coefficient*

Fig. 8 compares the computational results under various loading coefficients, with the condition of $L/D = 1.5$, $\phi = 4^\circ$ and $h/D = 0.5$ fixed. Note that in the corresponding experiments, wire-netting sheets were imposed as the load instead

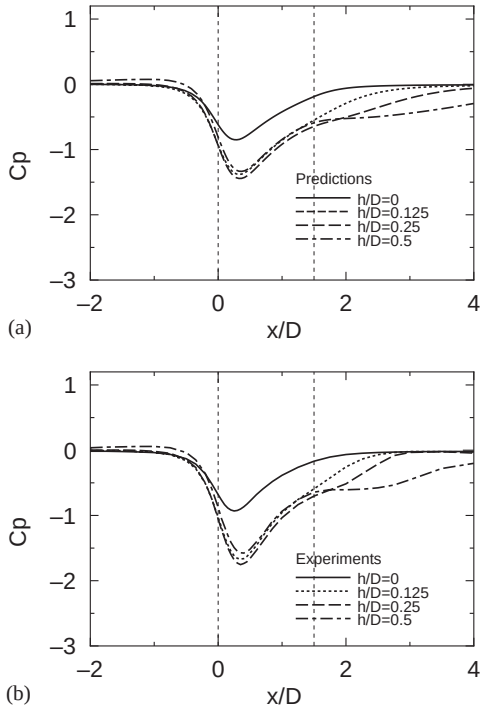

Fig. 7. Comparison of on-axis pressure coefficient ($L/D = 1.5$, $\phi = 4^\circ$, $C_t = 0$): (a) Predictions and (b) experiments.

of turbine blades [6]. In Fig. 8(b), the discontinuity in the pressure profile reflects the load, while the velocity varies continuously due to the restriction of the continuity equation. It is seen from the figure that the present computation returns generally reasonable trends for the variation of the loading coefficient, though its accuracy is not perfect. As the loading coefficient increases, the maximum velocity decreases and the discontinuity in the pressure profile becomes larger. It is interesting that even the case of $C_t = 0.9$ still provides a high level of the maximum velocity around 1.0, which can never be achieved by a bare wind turbine.

Fig. 9 compares the characteristic values for the condition of $L/D = 1.5$ and $\phi = 4^\circ$. Characteristic values investigated are acceleration factor ($K = U_1/U_0$), input-power coefficient ($C_p^* = C_t K^3$), base-pressure coefficient ($C_{pb} = (P_b - P_0)/(\frac{1}{2}\rho U_0^2)$) and pressure-recovery coefficient ($C_{pd} = (P_b - P_2)/(\frac{1}{2}\rho U_2^2)$). Note that $h/D = 0$ in the figure denotes a diffuser with no flange. As seen in the figure, the present results are in generally good agreement with the corresponding experimental data, though a slight difference is seen. From these results, it is shown that the present computation has the capability of predicting such complex flow fields even under conditions with a load inside the diffuser.

From the figures, some interesting and important knowledge can be obtained. As for the C_{pd} profiles in Fig. 9(d), even with a load inside the diffuser, there is not large

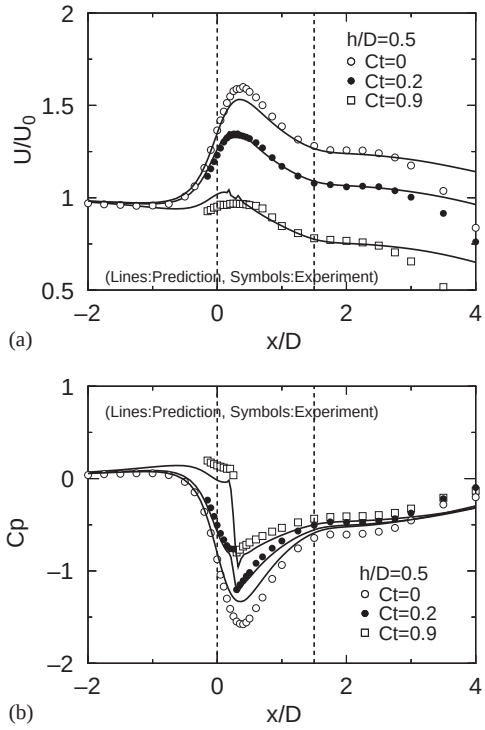

Fig. 8. Comparison of on-axis distributions ($L/D = 1.5$, $\phi = 4^\circ$, $h/D = 0.5$): (a) Streamwise velocity and (b) pressure coefficient.

difference among all the cases regardless of the existence of a flange. This fact supports the aforementioned explanation that the deceleration mechanism inside a diffuser is similar, so long as the same diffuser shape is used. From the one-dimensional design theory of a flanged diffuser by Inoue et al. [7], the best performance is obtained under the condition as

$$C_t = 2(1 - C_{pd}). \tag{8}$$

Note that in Eq. (8), C_t is determined as $C_t = (P_1 - P_2)/(\frac{1}{2}\rho U_2^2)$ and corresponds to Eq. (7) under the present computational condition. In Fig. 9(d), C_{pd} is roughly 0.4–0.5 and thus the best C_t is estimated to be 1.0–1.2 by using Eq. (8). Having considered that the best performance for a bare wind turbine is obtained at $C_t = 2$, the value of C_t presently estimated is considerably smaller than that for a bare wind-turbine case. From Fig. 9(b), it is confirmed that the highest performance is actually achieved at $C_t = 1.0-1.2$.

Also is shown that C_{pb} with a flange is maintained at a constant level with small range of variation, regardless of the operating condition (C_t). This indicates that the existence of a flange is a very strong boundary condition to determine the flow behind the flange and also periphery of the diffuser. Owing to this lower C_{pb}, a flanged diffuser draws wind much more than a diffuser with no flange does,

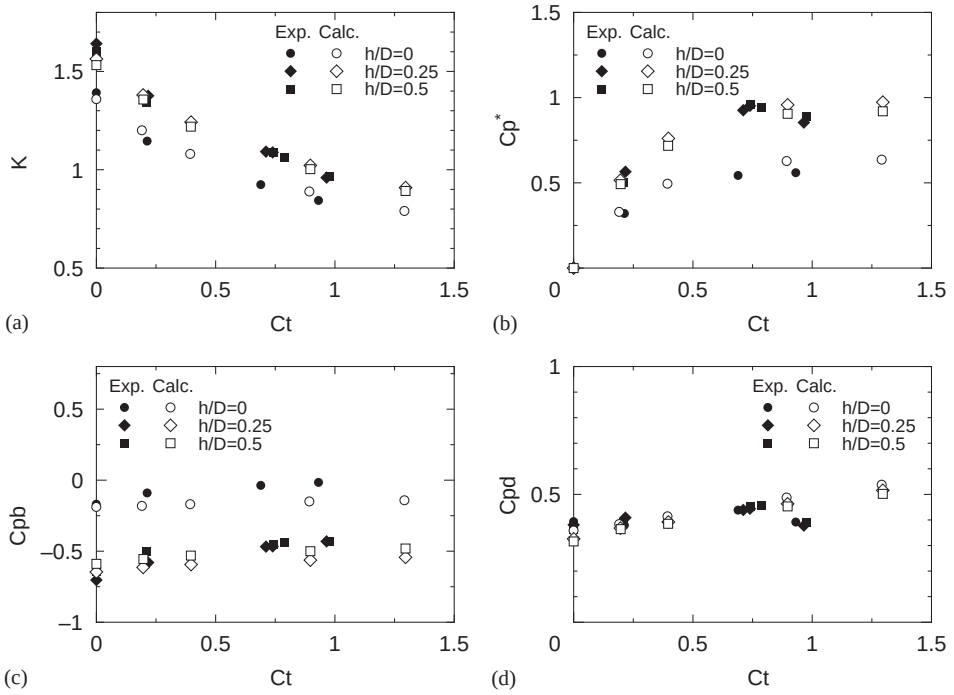

Fig. 9. Effect of loading coefficient on performance ($L/D = 1.5$, $\phi = 4^\circ$): (a) Acceleration factor; (b) input-power coefficient; (c) base-pressure coefficient and (d) pressure-recovery coefficient.

providing higher values of both K and C_p^*. The base-pressure coefficient C_{pb} is one of the important factors for the performance of a flanged diffuser [7] and thus the knowledge presently obtained is very useful for its further development.

3.3. Examination of larger opening angle

So far, it has been generally said that the optimum diffuser opening angle to prevent separation is around 4° for an axisymmetric diffuser. According to this fact, most test cases in this study were performed under the condition of $\phi = 4^\circ$. Recently, however, it has been elucidated that a wind turbine with flanged diffuser using a larger opening angle (10° or more) can provide rather higher performance [16], though such a widely expanded diffuser usually suffers from separations caused by the strong adverse pressure gradient. To reveal unknown characteristics on this matter, computational results for a larger opening angle ($\phi = 15^\circ$) were compared with those of the other cases for $\phi = 4^\circ$.

Fig. 10 compares the characteristic values. In Fig. 10(b), the dotted line denotes the Betz limit ($C_p^* = 16/27$) and the results with no diffuser are also included for reference. It is clearly seen that the performance for the case of $\phi = 15^\circ$ shows a special trend. In the lower C_t (<0.7) range, its performance is not so high, rather

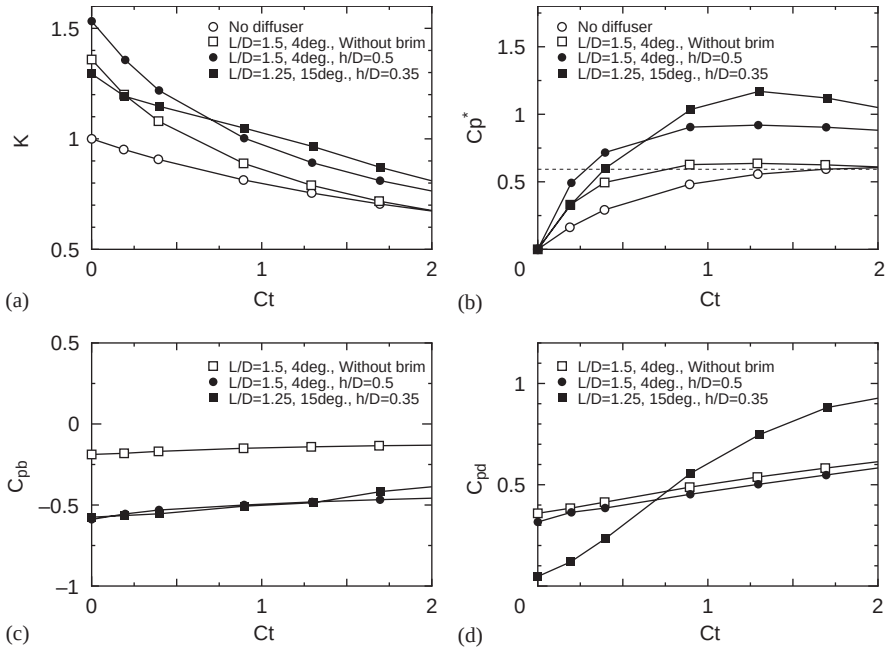

Fig. 10. Effect of diffuser opening angle on performance: (a) Acceleration factor; (b) input-power coefficient; (c) base-pressure coefficient and (d) pressure-recovery coefficient.

inferior to that for the case of $\phi = 4^\circ$ $(h/D = 0.5)$. As the loading coefficient increases ($C_t > 0.7$), however, the performance for $\phi = 15^\circ$ becomes higher, reaching the highest performance at $C_t = 1.3$. Similar trends are seen in the behavior of both the acceleration factor (K) and the pressure-recovery coefficient (C_{pd}). In contrast to such a special trend, however, there is not so large difference regarding C_{pb} between the cases of $\phi = 15^\circ$ $(h/D = 0.35)$ and $\phi = 4^\circ$ $(h/D = 0.5)$. It is confirmed again that the existence of a flange is a very strong boundary condition to determine the peripheral flow.

To investigate the cause of such a special trend for $\phi = 15^\circ$, streamlines for three different loading coefficients ($C_t = 0, 0.4, 1.3$) are compared in Fig. 11. The flow detaches at the inlet of the diffuser for all three cases. However, the separated streamline shows different trends between the case of $C_t = 1.3$ and the other two cases. In the lower C_t cases (i.e. $C_t = 0, 0.4$), the separated streamline does not reattach the inside wall and then a massive separation is generated all over the near-wall region inside the diffuser. On the other hand, in the case of $C_t = 1.3$, the separated streamline reattaches the inside wall soon after separation, owing to which the flow goes along the wall with no massive separation generated downstream. This also enables the flow to expand effectively and then a high level of C_{pd} is maintained, leading to a higher acceleration factor (K) as shown in Fig. 10(a). Such being the case, the performance of a flanged diffuser strongly depends on the fact whether there exists a separation inside the diffuser. Also, the loading coefficient has strong

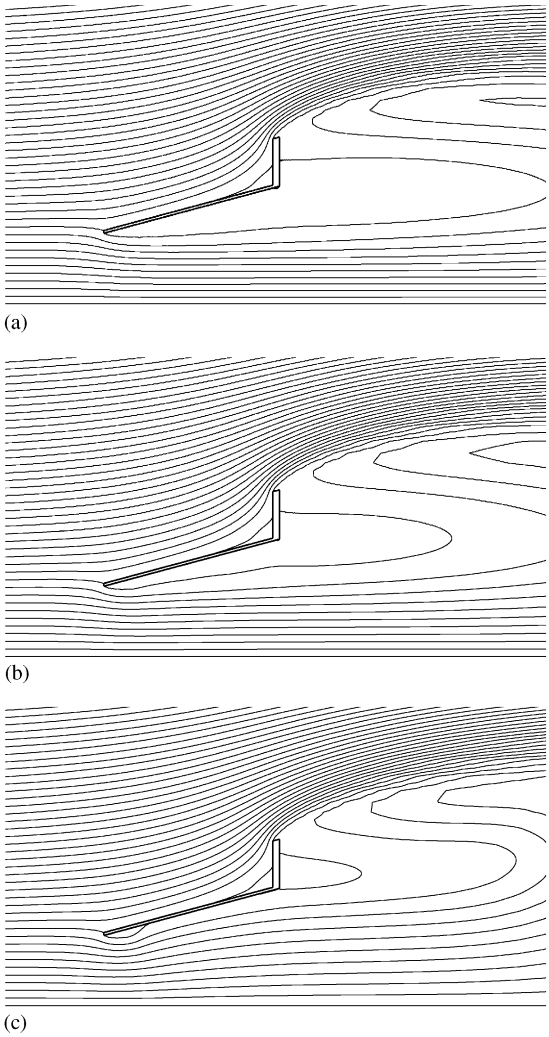

Fig. 11. Comparison of streamlines for various loading coefficients ($L/D = 1.25,\ \phi = 15^\circ,\ h/D = 0.35$): (a) $C_t = 0$; (b) $C_t = 0.4$ and (c) $C_t = 1.3$.

relationship with the generation of a separation. This suggests that the performance of a flanged diffuser needs to be discussed under conditions with suitable loading coefficient.

From these results, it is confirmed that a flanged diffuser even with a larger opening angle (10° or more) has a possibility of reaching the highest performance, so long as the flow inside the diffuser is successfully controlled not to cause any separation. This fact is a notable feature of a flanged-diffuser flow and very useful information for its optimum design.

4. Concluding remarks

Numerical investigations were carried out for flow fields around flanged diffusers to develop small-type wind turbines under 1.5 kW. The main conclusions derived from the study are as follows:

- Computational results were in good agreement with the corresponding experimental data. It has been confirmed from this fact that the present computational procedure is very useful to investigate flow fields of this kind.
- Design concept for a wind turbine with flanged diffuser is considerably different from that for a normal one. The local loading coefficient for the best performance of a flanged diffuser is considerably smaller than that for a bare wind turbine.
- Performance of a flanged diffuser strongly depends on the fact whether there exists a separation inside the diffuser. Also, the loading coefficient has strong relationship with the generation of a separation. From these facts, the performance of a flanged diffuser needs to be discussed under conditions with suitable loading coefficient.
- The present investigation suggests that a relatively small loading coefficient, avoiding a separation and maintaining a high pressure-recovery coefficient, tends to give high performance for a wind turbine with flanged diffuser.

Acknowledgements

This work was supported by four Grant-in-Aids for Scientific Research, No. 14205139, sponsored by the Ministry of Education, Culture, Sports, Science and Technology, Japan, for Environment Protection Research sponsored by Sumitomo Fund, for Fluid Machinery Research sponsored by Harada Memorial Fund and for the Program and Project for Education and Research of Kyushu University. It was also supported by a matching fund of the Ministry of Economy, Trade and Industry. KA wishes to express his appreciation to Professor M.A. Leschziner of Imperial College of Science, Technology and Medicine, London, UK for the support in using the STREAM code.

References

[1] O. Igra, Research and development for shrouded wind turbines, Energy Convers. Manage. 21 (1981) 13–48.
[2] B.L. Gilbert, K.M. Foreman, Experiments with a diffuser-augmented model wind turbine, Trans. ASME, J. Energy Resour. Technol. 105 (1983) 46–53.
[3] M. Nagai, K. Irabu, Momentum theory for diffuser augmented wind turbine, Trans. JSME 53–489 (1987) 1543–1547 (in Japanese).
[4] D.G. Phillips, P.J. Richards, R.G.J. Flay, CFD modelling and the development of the diffuser augmented wind turbine, Proceedings of the Computational Wind Engineering 2000, Birmingham, 2000, pp. 189–192.
[5] I. Ushiyama, Introduction of Wind Turbine, Sanseido Press, Tokyo, 1997, pp. 77–84 (in Japanese).

[6] Y. Ohya, T. Karasudani, A. Sakurai, M. Inoue, Development of shrouded wind turbine with brimmed diffuser, J. Wind Eng. Ind. Aerodyn., submitted.
[7] M. Inoue, A. Sakurai, Y. Ohya, A simple theory of wind turbine with a brimmed diffuser, Turbomachinery 30 (8) (2002) 497–502 (in Japanese).
[8] K. Abe, Y.J. Jang, M.A. Leschziner, An investigation of wall-anisotropy expressions and length-scale equations for non-linear eddy-viscosity models, Int. J. Heat Fluid Flow 24 (2003) 181–198.
[9] Y.-J. Jang, M.A. Leschziner, K. Abe, L. Temmerman, Investigation of anisotropy-resolving turbulence models by reference to highly-resolved LES data for separated flow, Flow Turbulence Combust. 69 (2002) 161–203.
[10] D.C. Wilcox, Reassessment of the scale-determining equation for advanced turbulence models, AIAA J. 26 (1988) 1299–1310.
[11] K. Abe, T. Kondoh, Y. Nagano, On Reynolds stress expressions and near-wall scaling parameters for predicting wall and homogeneous turbulent shear flows, Int. J. Heat Fluid Flow 18 (1997) 266–282.
[12] K. Abe, T. Kondoh, Y. Nagano, A new turbulence model for predicting fluid flow and heat transfer in separating and reattaching flows—I. flow field calculations, Int. J. Heat Mass Transfer 37 (1994) 139–151.
[13] F.S. Lien, M.A. Leschziner, A general non-orthogonal collocated finite volume algorithm for turbulent flow at all speeds incorporating second-moment turbulence-transport closure, Part 1: computational implementation, Comput. Methods Appl. Mech. Eng. 114 (1994) 123–148.
[14] D.D. Apsley, M.A. Leschziner, Advanced turbulence modelling of separated flow in a diffuser, Flow Turbulence Combust. 63 (2000) 81–112.
[15] F.S. Lien, M.A. Leschziner, Upstream monotonic interpolation for scalar transport with application to complex turbulent flows, Int. J. Num. Methods Fluids 19 (1994) 527–548.
[16] Y. Ohya, T. Karasudani, A. Sakurai, M. Inoue, N. Miura, Part 2—Development of high-performance wind turbine system by wind-lens effect (locally concentrated wind energy), Proceedings of the 24th Symposium on Wind Energy Utilization, Tokyo, 2002, pp. 165–168 (in Japanese).